EFFECT OF RHEOLOGICAL PARAMETERS ON DRAG-REDUCING TURBULENT BOUNDARY LAYER OF VISCOELASTIC FLUID

Shinji Tamano
Graduate School of Engineering,
Nagoya Institute of Technology
Gokiso-cho, Showa-ku, Nagoya, 466-8555, Japan
tamano.shinji@nitech.ac.jp

Motoyuki Itoh
Graduate School of Engineering,
Nagoya Institute of Technology
Gokiso-cho, Showa-ku, Nagoya, 466-8555, Japan
itoh.motoyuki@nitech.ac.jp

Kazuhiko Yokota
Graduate School of Engineering,
Nagoya Institute of Technology
Gokiso-cho, Showa-ku, Nagoya, 466-8555, Japan
yokota.kazuhiko@nitech.ac.jp

ABSTRACT

Direct numerical simulation of a zero-pressure gradient drag-reducing turbulent boundary layer of viscoelastic solutions was performed at momentum-thickness Reynolds number $Re_{\theta_0} = 500$ and Weissenberg number $We = 25$ using constitutive equation models such as the Oldroyd-B model and Giesekus model (the mobility factor $\alpha = 0.001, 0.002, 0.005, 0.01$) in which the rheological properties are different. It is found that the maximum drag reduction ratio $\%DR$ for the Oldroyd-B model is larger than that for the Giesekus model even at the same Weissenberg number ($We = 25$), although the maximum $\%DR$ for the Giesekus model approaches one for the Oldroyd-B model as α decreases from 0.01 to 0.001. For the Giesekus model with $\alpha = 0.001$, we can see that quasi-streamwise vortices are weakened and become larger in the streamwise direction, compared to the Giesekus model with $\alpha = 0.01$. The present results indicate that the higher elongational viscosity yields the larger drag reduction ratio, so that turbulence statistics and structures are modified more clearly in the drag-reducing turbulent boundary layer.

INTRODUCTION

Velocity measurements of a drag-reducing turbulent channel and pipe flows of viscoelastic fluids have yielded valuable knowledge about the suppression of turbulence, the modification of near-wall coherent structures, and the stress defect (e.g. Gyr and Bewersdorff, 1995; Warholic et al., 1999). On the other hand, there have been few studies on the drag-reducing effect for a turbulent boundary layer. Recently, White et al. (2004) and Itoh et al. (2005) have clarified the effects of polymer and surfactant additives on the turbulent boundary layer, respectively. However, the detailed mechanism of the drag reduction for the turbulent boundary layer flow of viscoelastic fluids has not been well understood.

In the last decade, there have been many direct numerical simulation (DNS) studies of drag-reducing turbulent channel flow (e.g. Sureshkumar et al., 1997; Min et al., 2003; Yu and Kawaguchi, 2004), while there are few DNS of turbulent boundary layer flow of viscoelastic fluids. Quite recently, Dimitropoulos et al. (2005, 2006) and Shin and Shaqfeh (2005) performed a DNS of a polymer-induced drag-reducing zero-pressure gradient turbulent boundary layer flow using the FENE-P model. Tamano et al. (2007) performed a DNS of a drag-reducing turbulent boundary layer of viscoelastic fluids using the Oldroyd-B and Giesekus models. However, it is quite insufficient compared to the DNS of drag-reducing turbulent channel flow.

In the present study, DNS of a zero-pressure gradient turbulent boundary layer of a drag-reducing viscoelastic fluid are performed using constitutive equation models such as the Oldroyd-B and Giesekus models in which the rheological properties are different.

NUMERICAL METHOD AND CONDITION

The non-dimensional governing equations for the incompressible viscoelastic flow are continuity and momentum equations:

$$\frac{\partial u_i}{\partial x_i} = 0, \tag{1}$$

$$\frac{\partial u_i}{\partial t} + \frac{\partial (u_i u_j)}{\partial x_j} = -\frac{\partial p}{\partial x_i} + \frac{1-\beta}{Re_{\theta_0}}\frac{\partial E_{ij}}{\partial x_j} + \frac{\beta}{Re_{\theta_0}}\frac{\partial^2 u_i}{\partial x_j \partial x_j}, \tag{2}$$

where u_i is the velocity component, p is pressure, x_i is spatial coordinate, t is time, and E_{ij} is the viscoelastic stress component. In this paper, x_1 (x), x_2 (y) and x_3 (z) directions are streamwise, wall-normal and spanwise, respectively. $\beta = \eta_s/\eta_0$ is the ratio of zero shear rate solvent viscosity η_s to solution viscosity η_0. For the Giesekus model, the non-dimensional constitutive equation for E_{ij} is as follows:

$$E_{ij} + We(\frac{\partial E_{ij}}{\partial t} + u_k \frac{\partial E_{ij}}{\partial x_k} - \frac{\partial u_i}{\partial x_k} E_{jk} - E_{ki} \frac{\partial u_j}{\partial x_k} + \alpha E_{jk} E_{ki})$$
$$= \frac{\partial u_i}{\partial x_j} + \frac{\partial u_j}{\partial x_i}, \quad (3)$$

where α is the mobility factor. The mobility factor α is from 0 to 1, and the Giesekus model with $\alpha = 0$ corresponds to the Oldroyd-B model (Bird et al., 1987).

The inflow condition for the boundary layer is given by the method proposed by Lund et al. (1998), so that the computational domain is divided into the main and driver parts. The computational parameters are the momentum-thickness Reynolds number and the Weissenberg number which are defined as follows:

$$Re_{\theta_0} = \frac{\rho U_e \theta_0}{\eta_0}, \quad (4)$$

$$We = \frac{\lambda U_e}{\theta_0}, \quad (5)$$

where U_e is the free-stream velocity, θ_0 is the momentum-thickness at the inlet plane of the driver part, η_0 is the zero-shear viscosity of the solution, ρ is density, and λ is the relaxation time.

The second-order accurate finite difference scheme on a staggered grid is used. The velocity components are discretized on the grid cell edges, whereas the pressure and all the components of viscoelastic stress tensors E_{ij} are defined at the center of each cell. The coupling algorithm of the discrete continuity and momentum equations (1) and (2) is based on the second-order splitting method. The resulting discrete Poisson equation for the pressure is solved using the SOR method after FFT in the periodic (z) direction. The second-order upwind difference scheme is used for the polymer-stress convection term, and an artificial diffusion is added in (3) to prevent the numerical instability (Sureshkumar et al., 1997). The semi-implicit time marching algorithm is used where the diffusion term in the wall-normal direction is treated implicitly with the Crank–Nicolson scheme, and the third-order Runge–Kutta scheme is used for all other terms.

The boundary conditions for the computational domain are the same as those of Lund et al. (1998). The momentum-thickness Reynolds number Re_{θ_0} is 500 and the Weissenberg number We is 25. The size of the computational domain is equal to $(L_x \times L_y \times L_z) = (200\theta_0 \times 30\theta_0 \times 20\pi\theta_0/3)$ in the streamwise, wall-normal, and spanwise directions, respectively. The grid size is $(N_x \times N_y \times N_z) = (256 \times 64 \times 64)$. The grid spacing in x and z directions is uniform, and the wall-normal grids are given by a hyperbolic tangent stretching function. The grid resolution is evaluated by $\Delta x_i^+ = \Delta x_i u_\tau/\nu_0$ $(i = 1, 2, 3)$, where Δx_i is the grid spacing in the x_i direction, u_τ is the friction velocity at the inlet of main part, and $\nu_0 = \eta_0/\rho$ is the zero-shear kinematic viscosity of the solution. The viscosity ratio β is fixed at 0.9 for the turbulent boundary layer of dilute viscoelastic fluids. The mobility factor α for the Giesekus model is 0.001, 0.002, 0.005, and 0.01. Here, the mobility factor α is related to the extensibility of the polymer chains, i.e., the smaller mobility factor corresponds to the larger elongational viscosity. Generally, the Giesekus model represents the shear-thinning property and the moderate elongational viscosity, while the Oldroyd-B model represents the constant shear viscosity and the higher elongational viscosity (Bird et al., 1987). The present turbulence statistics are obtained by averaging over

Table 1: Numerical and physical conditions

	Newtonian	Oldroyd-B	Giesekus
Re_{θ_0}	500	500	500
We	–	25	25
N_x	256	256	256
N_y	64	64	64
N_z	64	64	64
L_x	$200\theta_0$	$200\theta_0$	$200\theta_0$
L_y	$30\theta_0$	$30\theta_0$	$30\theta_0$
L_z	$20\pi\theta_0/3$	$20\pi\theta_0/3$	$20\pi\theta_0/3$
Δx^+	20	20	20
$\Delta y^+_{min} - \Delta y^+_{max}$	$0.38 - 36$	$0.38 - 36$	$0.37 - 36$
Δz^+	8.5	8.4	8.3
β	1.0	0.9	0.9
α	–	0	0.001, 0.002, 0.005, 0.01
$\Delta t U_e/\theta_0$	0.02	0.008	0.008

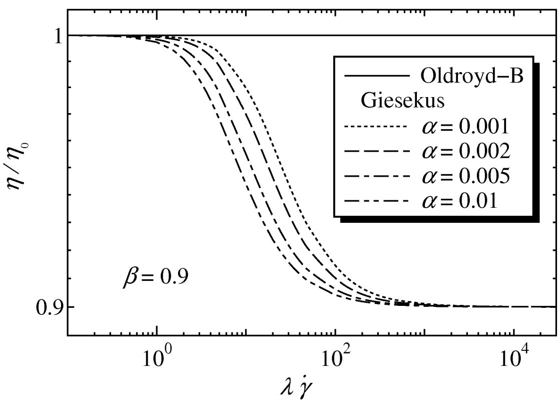

Figure 1: Shear viscosity for steady shear flow.

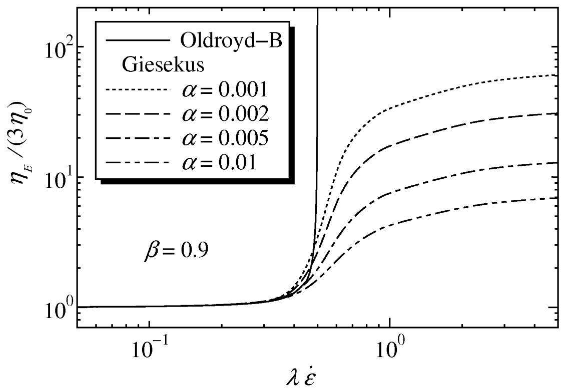

Figure 2: Extensional viscosity for steady elongational flow.

space (spanwise direction) and time of over $1000\theta_0/U_e$ after the turbulent flow becomes stationary, where the time increment $\Delta t U_e/\theta_0$ is 0.008 for the Oldroyd-B and Giesekus models and 0.02 for Newtonian fluid. In this paper, $\overline{}$ and $'$ represent the time–space (spanwise direction) average and the deviation, respectively. The superscript $^+$ represents the variables normalized by wall variables. The physical and numerical parameters for all cases are given in table 1. Readers would be referred to the related study (Tamano et al., 2007) in terms of details of the numerical method and conditions.

RHEOLOGICAL PROPERTIES

For the steady shear flow, the non-dimensional shear vis-

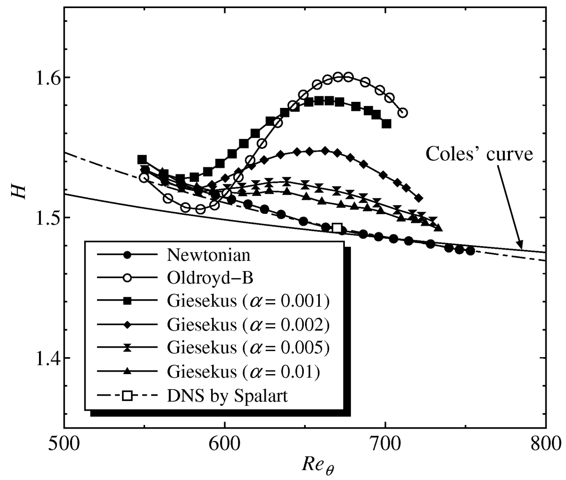

Figure 3: Shape factor versus Reynolds number.

cosity η/η_0 for the Oldroyd-B and Giesekus models is defined as follows (see Bird et al., 1987):

$$\frac{\eta}{\eta_0} = 1, \tag{6}$$

$$\frac{\eta}{\eta_0} = (1-\beta)\frac{(1-n_2)^2}{1+(1-2\alpha)n_2} + \beta, \tag{7}$$

where

$$n_2 = \frac{1-\Lambda}{1+(1-2\alpha)\Lambda}, \tag{8}$$

$$\Lambda^2 = \frac{\sqrt{1+16\alpha(1-\alpha)\kappa^2}-1}{8\alpha(1-\alpha)\kappa^2}. \tag{9}$$

For the Giesekus model, the shear viscosity η/η_0 depends on the nondimensional shear rate $\kappa = \lambda\dot{\gamma}$. Figure 1 shows the profile of the shear viscosity η/η_0 for the steady shear flow at $\beta = 0.9$. The value of η/η_0 for the Giesekus model decreases with the increase of the shear rate $\lambda\dot{\gamma}$ in the region $10^0 < \lambda\dot{\gamma} < 10^4$, and approaches a constant value ($= 0.9$) for $\lambda\dot{\gamma} > 10^4$. For the Oldroyd-B model, the shear viscosity η/η_0 is independent of the shear rate ($\eta/\eta_0 = 1$).

For the steady elongational flow, the non-dimensional elongational viscosity $\eta_E/(3\eta_0)$ for the Oldroyd-B and Giesekus models are defined as follows (see Bird et al., 1987):

$$\frac{\eta_E}{3\eta_0} = \beta + (1-\beta)\frac{1}{(1+\xi)(1-2\xi)}, \tag{10}$$

$$\frac{\eta_E}{3\eta_0} = \frac{(1-\beta)}{6\alpha\xi}\left(3\xi + \sqrt{1-4(1-2\alpha)\xi+4\xi^2} - \sqrt{1+2(1-2\alpha)\xi+\xi^2}\right) + \beta, \tag{11}$$

where $\xi = \lambda\dot{\varepsilon}$ is the non-dimensional elongational rate. Figure 2 shows the profile of the extensional viscosity $\eta_E/(3\eta_0)$ for the steady elongational flow at $\beta = 0.9$. For the Oldryod-B model, $\eta_E/(3\eta_0)$ is almost unity for $\lambda\dot{\varepsilon} < 0.5$, and is infinity at $\lambda\dot{\varepsilon} = 0.5$. For the Giesekus model, $\eta_E/(3\eta_0)$ for $\lambda\dot{\varepsilon} > 0.5$ becomes larger with the smaller mobility factor α.

RESULTS AND DISCUSSIONS

Boundary Layer Parameters

Figure 3 shows the dependence of the shape factor $H = \delta^*/\delta$ on the momentum-thickness Reynolds number Re_θ. $\delta = \delta_{99.5}$ and δ^* are the boundary layer thickness and the boundary layer displacement thickness, respectively.

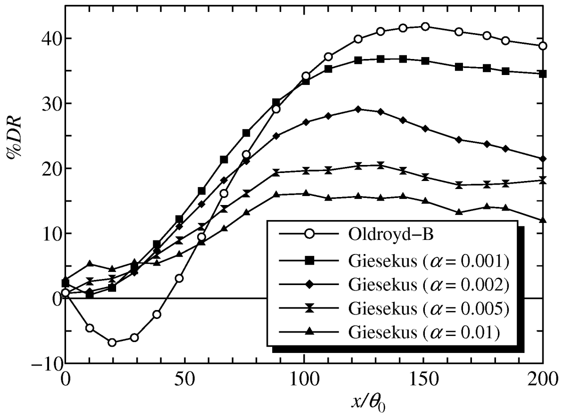

Figure 4: Streamwise variation of drag reduction ratio.

Table 2: Drag reduction ratio

	Oldroyd-B	Giesekus			
α		0.001	0.002	0.005	0.01
$\%DR_{x/\theta_0=19.53}$	−6.79	0.53	1.07	2.62	4.45
$\%DR_{x/\theta_0=100.8}$	34.2	33.4	27.1	19.4	16.1
$\%DR_{x/\theta_0=164.8}$	41.0	35.6	24.4	17.4	13.2

In the figure, the dot–dashed line represents the DNS data of Spalart (1988) and the solid line represents Coles' curve (Coles, 1962) for the Newtonian fluid. The data of H for Newtonian fluid agree well with data of Spalart. Near the inlet region ($550 \leq Re_\theta \leq 600$), the value of H for the Oldroyd-B model is smaller than that for Newtonian fluid, while for $Re_\theta > 600$, H for the Oldroyd-B model drastically increases with the increase of Re_θ and reaches the maximum at $Re_\theta \simeq 670$, where H for the Oldroyd-B model is much larger than that for Newtonian fluid and ranges between the value for the laminar flow ($H = 2.59$) and the value for the turbulent flow of Newtonian fluid. On the other hand, H for the Giesekus model agrees well with that for Newtonian fluid in the region $550 \leq Re_\theta \leq 600$, which is independent of α, and it becomes closer to that for the Oldroyd-B model with decreasing α for $Re_\theta > 600$.

Drag Reduction Ratio

Figure 4 shows the streamwise variation of drag reduction ratio $\%DR$, which is defined as follows:

$$\%DR = \frac{C_{f,\ \mathrm{Newtonian}} - C_{f,\ \mathrm{Viscoelastic}}}{C_{f,\ \mathrm{Newtonian}}} \times 100, \tag{12}$$

where $C_f = 2(u_\tau/U_e)^2$ is the friction coefficient at the same streamwise positions. $\%DR$ for the Oldroyd-B model is negative and positive in the region $0 < x/\theta_0 < 50$ and for $x/\theta_0 > 50$, respectively. The increase of friction drag ($\%DR < 0$) near the inlet region may be due to the sudden change of velocity fields caused by the unfavorable effect of the inlet boundary condition in which the velocity field data of Newtonian fluid in the driver part is used (see Dimitropoulos et al., 2005; Tamano et al., 2007). The maximum drag reduction ratio ($\%DR = 42$) is observed at $x/\theta_0 = 150.8$ for the Oldroyd-B model. On the other hand, the drag reduction ratio for the Giesekus model with any mobility factors tested can be seen even near the inlet region, and gradually increases in the streamwise direction. It is found that the maximum $\%DR$ for the Oldroyd-B model is larger than that for the Giesekus model even at the same Weissenberg number ($We = 25$), although the maximum $\%DR$ for the

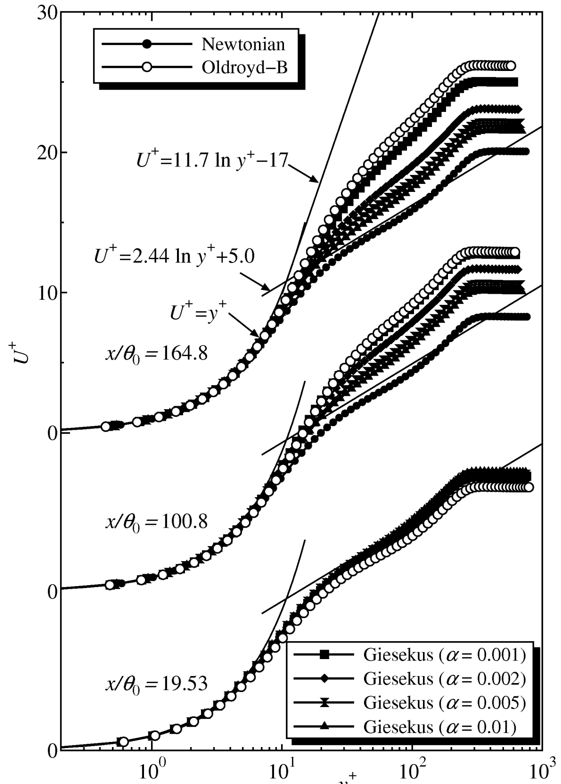

Figure 5: Mean velocity profiles.

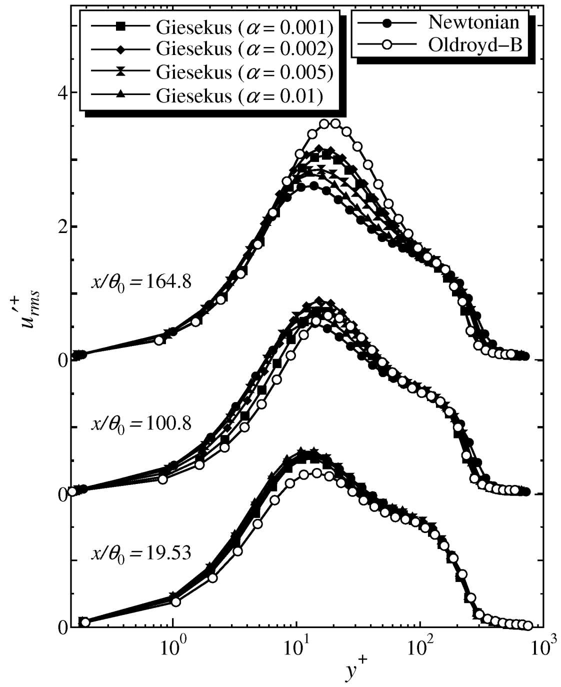

Figure 6: Profiles of streamwise turbulence intensity.

Giesekus model approaches one for the Oldroyd-B model as α decreases. This indicates that high elongational viscosity is important in order to obtain a large drag reduction ratio.

In this study, we obtained turbulence statistics at twenty different streamwise locations. The results at the locations of $x/\theta_0 = 19.53$ (upstream), $x/\theta_0 = 100.8$ (center), and $x/\theta_0 = 164.8$ (downstream) are presented below. The drag reduction ratios at these locations are summarized in table 2 for the Oldryod-B model and the Giesekus model ($\alpha = 0.001, 0.002, 0.005, 0.01$).

Mean Velocity Profile

Figure 5 shows the profiles of the mean velocity U^+. In the figure, the Virk's ultimate profile ($U^+ = 11.7 \ln y^+ - 17$) is presented (Virk, 1975). It is seen at $x/\theta_0 = 100.8$ and $x/\theta_0 = 164.8$ that U^+ for the Giesekus model shifts upward compared to Newtonian fluid and the magnitude of the shift becomes larger with the decrease of α, while U^+ for the Oldroyd-B model shifts upward compared to the Giesekus model with $\alpha = 0.001$. This means that the mean velocity shifts upward more as the amount of drag reduction ratio becomes larger, which is consistent with the previous experimental and numerical studies (e.g. Itoh et al., 2005; Dimitropoulos et al., 2005). For the Oldroyd-B model, the slope of the velocity profile in the log-law region at $x/\theta_0 = 164.8$ is steeper than that at $x/\theta_0 = 100.8$. At $x/\theta_0 = 19.53$, the profile of U^+ in the log-law region slightly shifts up and down for the Giesekus and Oldroyd-B models, respectively. This corresponds to the fact that the drag reduction ratio at $x/\theta_0 = 19.53$ is positive and negative for the Giesekus and Oldroyd-B models, respectively.

Turbulence Statistics

Distributions of the streamwise turbulence intensity u'^+_{rms} are shown in Fig. 6. The maximum u'^+_{rms} for the Oldroyd-B model is smaller, slightly larger, and much larger at $x/\theta_0 = 19.53$, $x/\theta_0 = 100.8$ and $x/\theta_0 = 164.8$, respectively, compared to Newtonian fluid. At $x/\theta_0 = 100.8$ and $x/\theta_0 = 164.8$, the value of y^+ at the maximum of u'^+_{rms} for the Oldroyd-B model is larger than that for Newtonian fluid, as reported in previous experimental and numerical studies on drag-reducing turbulent channel flow (e.g. Warholic et al., 1999; Sureshkumar et al., 1997; Min et al., 2003; Yu and Kawaguchi, 2004). This indicates that the buffer layer for the Oldroyd-B model is thicker than that for Newtonian fluid. On the other hand, u'^+_{rms} for the Giesekus model with lower drag reduction ratio is slightly larger than that for Newtonian fluid at $x/\theta_0 = 164.8$. Note that the maximum value of streamwise turbulence intensity for the turbulent boundary layer is dependent on the streamwise location, and it is not directly related to the amount of drag reduction (see Tamano et al., 2007).

Figure 7 shows distributions of the wall-normal turbulence intensity v'^+_{rms}. At $x/\theta_0 = 19.53$, v'^+_{rms} for the Oldroyd-B model is smaller in the region $5 \leq y^+ \leq 100$ than that for Newtonian fluid. At $x/\theta_0 = 100.8$ and $x/\theta_0 = 164.8$, the difference in v'^+_{rms} between the Oldroyd-B model and Newtonian fluid is more apparent, which indicates that the velocity fluctuation is considerably attenuated in the wall-normal direction. On the other hand, for the Giesekus model, v'^+_{rms} at $x/\theta_0 = 100.8$ and $x/\theta_0 = 164.8$ approaches one for the Oldroyd-B model with decreasing α, and approaches one for Newtonian fluid with increasing α.

Figure 8 shows distributions of RMS of the streamwise vorticity fluctuation $\omega'^+_{x\,rms}$. At any streamwise locations, $\omega'^+_{x\,rms}$ for the Oldroyd-B model is much smaller than that for Newtonian fluid at $y^+ < 100$, while it agrees well with that for Newtonian fluid at $y^+ > 100$. At $x/\theta_0 = 100.8$ and $x/\theta_0 = 164.8$, the maximum of $\omega'^+_{x\,rms}$ for the Oldroyd-B model appears at $y^+ \simeq 100$, and the wall-normal locations of the maximum move considerably away from the wall compared to the location for Newtonian fluid ($y^+ \simeq 20$). Note that the location of minimum $\omega'^+_{x\,rms}$ for the Oldroyd-B

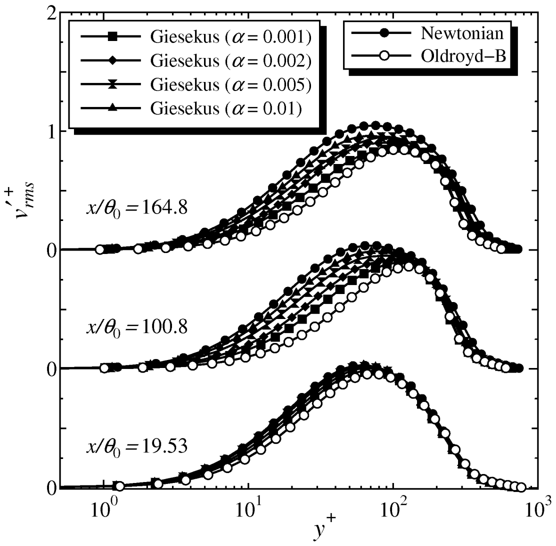

Figure 7: Profiles of wall-normal turbulence intensity.

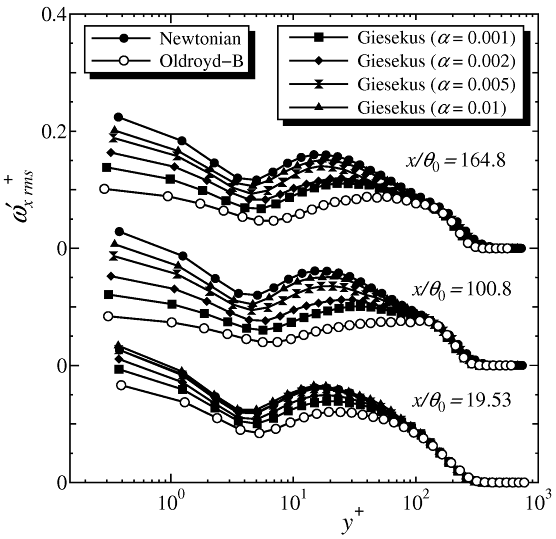

Figure 8: Profiles of streamwise vorticity fluctuation.

model ($y^+ \simeq 5$) is almost the same as that for Newtonian fluid. Here, it has been reported that the locations of the minimum and maximum of the RMS of streamwise vorticity fluctuation correspond to the average locations of lower limits and center of the quasi-streamwise vortices near the wall, respectively (Kim et al., 1987). Therefore, it can be deduced that the quasi-streamwise vortices become larger away from the wall, compared to Newtonian fluid. The same trend has also been reported in the drag-reducing turbulent channel flows (Dimitropoulos et al., 1998; Min et al., 2003), but the amount of the shift in the wall-normal direction observed in the present study is much larger. On the other hand, the profile of ω'^+_{xrms} for the Giesekus model ranges between ones for the Oldroyd-B model and Newtonian fluid at any streamwise locations, and becomes closer to one for Oldroyd-B model with the decrease of α.

Figure 9 shows distributions of the trace of mean viscoelastic stress $\overline{E_{kk}}^+$ which represents the magnitude of the polymer elongation (Min et al., 2003). At any streamwise locations, $\overline{E_{kk}}^+$ for the Oldroyd-B model is larger than that for the Giesekus model with any mobility factors in the region $1 \le y^+ \le 50$. From this result, it can be deduced that turbulence statistics are strongly affected by the high elongational viscosity, and the effect appears significantly in the region of center to downstream. Note that in the region very close to the wall ($y^+ < 1$), at $x/\theta_0 = 100.8$ and $x/\theta_0 = 164.8$, $\overline{E_{kk}}^+$ for the Giesekus model increases with the decrease of α and is larger than that for the Oldroyd-B model.

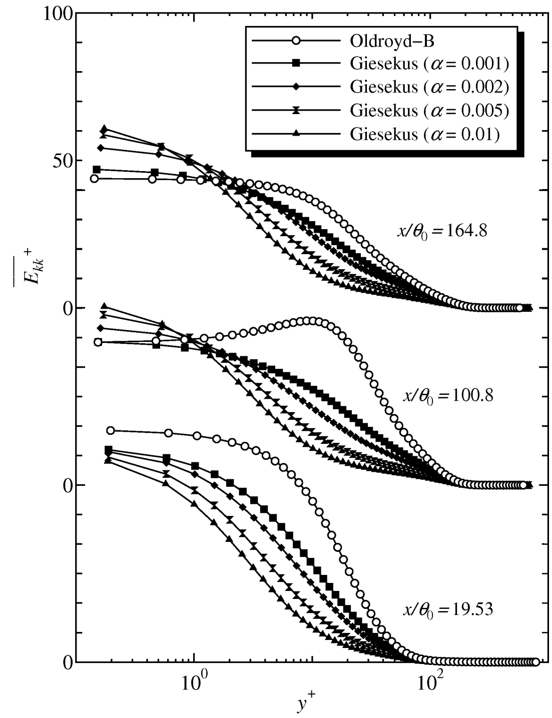

Figure 9: Trace of mean viscoelastic stress.

Turbulence Structures

Figure 10 shows the isosurface of the second invariant of velocity gradient tensor $Q\theta_0^2/U_e^2 = 0.005$ for the Giesekus model with $\alpha = 0.01$ and 0.001. The region in which the second invariant $Q = -(\partial u_i/\partial x_j)(\partial u_j/\partial x_i)/2$ is positive represents the region in which the strength of rotation overcomes the strain rate, and corresponds to the region where the vortices exist (Dubief and Delcayre, 2000). In the figure, the flow is from left to right, and the black area represents the wall. For the Giesekus model with $\alpha = 0.01$, there are numerous quasi-streamwise vortices near the wall in the region from the inlet to outlet, which is similar to that for Newtonian fluid (see Tamano, 2007). On the other hand, for the Giesekus model with $\alpha = 0.001$, only a few quasi-streamwise vortices can be seen for $x/\theta_0 > 50$, which is similar to that for the Oldroyd-B model (see Tamano, 2007). As shown in Fig. 9, the trace of mean viscoelastic stress $\overline{E_{kk}}^+$ for the Giesekus model becomes larger with the decrease of α and approaches that of the Oldroyd-B model in the region $1 \le y^+ \le 50$. Therefore, we can assume that near-wall coherent structures are strongly affected by the high elongational viscosity, and the effect appears significantly for $x/\theta_0 > 50$, in which the quasi-streamwise vortices are weakened and become larger in the streamwise direction.

CONCLUSIONS

Direct numerical simulation of a zero-pressure gradient drag-reducing turbulent boundary layer of viscoelastic solutions was performed at momentum-thickness Reynolds

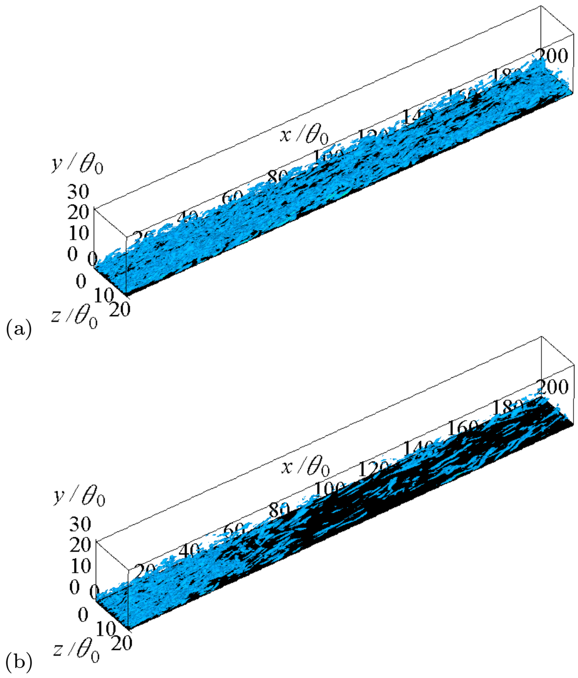

Figure 10: Isosurface of second invariant of velocity gradient tensor ($Q\theta_0^2/U_e^2 = 0.005$) for Giesekus model. Flow is from left to right: (a) $\alpha = 0.01$, and (b) $\alpha = 0.001$.

number $Re_{\theta_0} = 500$ and Weissenberg number $We = 25$ using constitutive equation models such as the Oldroyd-B model and Giesekus model (the mobility factor $\alpha = 0.001, 0.002, 0.005, 0.01$). The main results of the present study may be summarized as follows.

(1) The maximum drag reduction ratio $\%DR$ for the Oldroyd-B model is larger than that for the Giesekus model even at the same Weissenberg number ($We = 25$), although the maximum $\%DR$ for the Giesekus model approaches one for the Oldroyd-B model as α decreases from 0.01 to 0.001.

(2) At $x/\theta_0 = 100.8$ and $x/\theta_0 = 164.8$, the mean velocity U^+ for the Giesekus model shifts upward compared to Newtonian fluid and the magnitude of the shift becomes larger with the decrease of α, while U^+ for the Oldroyd-B model shifts upward compared to the Giesekus model with $\alpha = 0.001$.

(3) The profile of RMS of the streamwise vorticity fluctuation $\omega'^{+}_{x rms}$ for the Giesekus model ranges between ones for the Oldroyd-B model and Newtonian fluid at any streamwise locations, and becomes closer to one for Oldroyd-B model with the decrease of α.

(4) At any streamwise locations, the trace of mean viscoelastic stress $\overline{E_{kk}}^{+}$ which represents the magnitude of the polymer elongation for the Oldroyd-B model is larger than that for the Giesekus model with any mobility factors in the region $1 \le y^+ \le 50$.

(5) Quasi-streamwise vortices for the Giesekus model with $\alpha = 0.001$ are weakened and become larger in the streamwise direction, compared to those for the Giesekus model with $\alpha = 0.01$.

ACKNOWLEDGMENTS

We are grateful to Mr. S. Hotta for the assistance with the numerical simulations.

REFERENCES

Bird R. B., Armstrong R. C., and Hassager O., 1987, "Dynamics of Polymeric Liquids, Vol. 1: Fluid Mechanics, 2nd ed.", Wiley Interscience.

Coles D. E., 1962, "A manual of experimental boundary-layer practice for low-speed flow", *Rand Rep. Appendix A*, R-403-PR.

Dimitropoulos C. D., Sureshkumar R., and Beris A. N., 1998, "Direct numerical simulation of viscoelastic turbulent channel flow exhibiting drag reduction: effect of the variation of rheological parameters", *J. Non-Newtonian Fluid Mech.*, Vol. 79, pp. 433-468.

Dimitropoulos C. D., Dubief Y., Shaqfeh E. S. G., Moin P., and Lele S. K., 2005, "Direct numerical simulation of polymer-induced drag reduction in turbulent boundary layer flow," *Phys. Fluids*, Vol. 17, No. 011705.

Dimitropoulos C. D., Dubief Y., Shaqfeh E. S. G., and Moin P., 2006, "Direct numerical simulation of polymer-induced drag reduction in turbulent boundary layer flow of inhomogeneous polymer solutions", *J. Fluid Mech.*, Vol. 566, pp. 153-162.

Dubief Y., and Delcayre F., 2000, "On coherent-vortex identification in turbulence", *J. Turbulence*, Vol. 1, No. 11, pp. 1-22.

Gyr A., and Bewersdorff H.-W., 1995, "Drag Reduction of Turbulent Flows by Additives", Kluwer, Dordrecht, the Netherlands.

Itoh M., Tamano S., Yokota K., and Ninagawa M., 2005, "Velocity measurement in turbulent boundary layer of drag-reducing surfactant solution," *Phys. Fluids*, Vol. 17, No. 075107.

Kim J., Moin P., and Moser R., 1987, "Turbulence statistics in fully developed channel flow at low Reynolds number," *J. Fluid Mech.*, Vol. 177, pp. 133-166.

Lund T. S., Wu X., and Squires K. D., 1998, "Generation of turbulent inflow data for spatially-developing boundary layer simulations," *J. Comp. Phys.*, Vol. 140, pp. 233-258.

Min T., Yoo J. Y., Choi H., and Joseph D. D., 2003, "Drag reduction by polymer additives in a turbulent channel flow," *J. Fluid Mech.*, Vol. 486, pp. 213-238.

Shin M., and Shaqfeh E. S. G., 2005, "Viscoelastic turbulent boundary layer with near-wall injection of polymer molecules," *Annual Research Briefs 2005, Center for Turbulence Research*, NASA Ames/Stanford Univ., pp. 389-405.

Spalart, P. R., 1988, "Direct simulation of a turbulent boundary layer up to $Re_\theta = 1410$", *J. Fluid Mech.* Vol. 187, pp. 61-98.

Sureshkumar R., Beris A. N., and Handler R. A., 1997, "Direct numerical simulation of the turbulent channel flow of a polymer solution," *Phys. Fluids*, Vol. 9, pp. 743-755.

Tamano S., Itoh M., Hoshizaki K., and Yokota K., 2007, "Direct numerical simulation of drag-reducing turbulent boundary layer of viscoelastic fluid", *Phys. Fluids*, submitted.

Virk P. S., 1975, "Drag reduction fundamentals", *AIChE J.*, Vol. 21 (4), pp. 625-656.

Warholic M. D., Schmidt G. M., and Hanratty T. J., 1999, "The influence of a drag-reducing surfactant on a turbulent velocity field," *J. Fluid Mech.*, Vol. 388, pp. 1-20.

White C. M., Somandepalli V. S. R., and Mungal M. G., 2004, "The turbulence structure of drag-reduced boundary layer flow," *Exp. Fluids*, Vol. 36, pp. 62-69.

Yu B., and Kawaguchi Y., 2004, "Direct numerical simulation of viscoelastic drag-reducing flow: a faithful finite different method," *J. Non-Newtonian Fluid Mech.*, Vol. 116, pp. 431-466.